This is the accepted manuscript made available via CHORUS. The article has been published as:

Effective Control of the Charge and Magnetic States of Transition-Metal Atoms on Single-Layer Boron Nitride

Bing Huang, Hongjun Xiang, Jaejun Yu, and Su-Huai Wei

Phys. Rev. Lett. **108**, 206802 — Published 14 May 2012

DOI: 10.1103/PhysRevLett.108.206802

Effective Control of the Charge and Magnetic States of Transition-metal Atoms on Single-layer Boron-nitride

Bing Huang[1], Hongjun Xiang[2], Jaejun Yu[3], and Su-Huai Wei[1]

[1]*National Renewable Energy Laboratory,*

1617 Cole Boulevard, Golden, CO 80401, USA

[2]*Key Laboratory of Computational Physical Sciences and Department of Physics,*

Fudan University, Shanghai 200433, P. R. China and

[3]*Center for Strongly Correlated Materials Research,*

Department of Physics and Astronomy,

Seoul National University, Seoul 151-747, Korea

(Dated: February 16, 2012)

Abstract

Developing approaches to effectively control the charge and magnetic states is critical to the use of magnetic nanostructures in quantum information devices but is still challenging. Here we suggest that the magnetic and charge states of transition-metal (TM) doped single-layer boron-nitride (SLBN) systems can be easily controlled by the (internal) defect engineering and (external) electric fields (E_{ext}). The relative positions and symmetries of the in-gap levels induced by defect engineering and the TM *d*-orbital energy levels effectively determine the charge states and magnetic properties of the TM/SLBN system. Remarkably, the application of an E_{ext} can easily control the size of the crystal field splitting of the TM *d* orbitals and thus, leading to the spin crossover in TM/SLBN, which could be used as E_{ext}-driven non-volatile memory devices. Our conclusion got from TM/SLBN is valid generally in other TM adsorbed layered semiconductors.

Graphene has many interesting electronic and magnetic properties. Its low-dimensional nature makes it ideally suitable for nanoscale device applications[1]. In particular, graphene has been considered as a promising host material for spintronic related applications because it can posses magnetic moments through defect control such as forming nano ribbons[2, 3] or forming vacancies[4], and more importantly, it has low intrinsic spin-orbit interaction and low hyperfine interaction between the electron spins and the carbon nuclei. However, the coupling between the $2p$-like magnetic moments through electron or hole carriers, a central requirement of spintronics, is relatively weak. As a result, introducing transition metals (TM) in graphene system has become a popular choice to enhance the magnetic interactions.

Extensive experimental[5–7] and theoretically studies [8–11] have been carried out to test this idea. Indeed, magnetic properties of TM doped graphene can be significantly modified. However, because of the lack of band gap in graphene, the TM d orbitals strongly couples with the conduction or valence bands of graphene[10, 11] and further control of the charge and magnetic states of TM/graphene system is quite difficult[7], but the reliable control of the charge and magnetic states of a magnetic material is a key step for spintronics and quantum information devices[12, 13]. Naturally, one may expect to solve this difficulty by replacing metallic graphene layer with some semiconducting layers. Single-layer boron-nitride (SLBN) or other III-V (e.g., AlN and GaN) and II-VI (e.g., ZnO and ZnS) graphiticlike structures have been synthesized in experiments[14, 15] or predicted in theories[16, 17]. Owing to the large chemical difference between cation and anion atoms, these ionic layer structures display large heteropolar band gaps[14, 17]. Because the energies of TM $3d$ orbitals can exist inside the band gap[18], i.e., not in the conduction or valence band as in the case of TM/graphene, we expect that these in-gap TM $3d$ orbitals may be easier to be controlled by various approaches and the TM/III-V or TM/II-VI layer systems might be considered as preferential magnetic materials for low-dimensional spintronics.

In order to examine the controllability of the magnetic and charge states in these TM/III-V or TM/II-VI layer structures, taking TM/SLBN as a typical example, we have systematically studied $3d$ TM atoms (from Sc to Zn) doped SLBN based on density-functional theory (DFT) calculations[19]. In general, we find that the magnetic and charge states of TM/SLBN systems can be effectively controlled by the (internal) defect engineering and/or (external) electric fields (E_{ext}). The relative position and symmetry of the in-gap levels

induced by structural defects or impurities play a crucial role in determining the charge states and magnetic properties of adsorbed TM atoms. Interestingly, we show that an E_{ext} can effectively control the size of the crystal field splitting of the TM $3d$ orbitals, thus leading to a spin crossover effect in TM/SLBN system, which could be used for applications such as non-volatile memory. Our further calculations show that the conclusions got from TM/SLBN system are valid in other TM/III-V or TM/II-VI layer systems.

An isolated TM atom usually has $s^{1\uparrow}s^{1\downarrow}\ d^{m\uparrow}d^{n\downarrow}$ configuration, except for Cr and Cu atoms, where only one electron occupy the $4s$ orbital. After adsorption on pristine SLBN, the large Coulomb repulsion between the TM $4s$ orbital and the SLBN layer pushes up the $4s$ orbital energy, therefore can causes a charge transfer from TM $4s$ orbital to $3d$ orbital, resulting usually either in $d^{m+1\uparrow}s^{1\uparrow}d^{n\downarrow}s^{0\downarrow}$ (m $<$ 5) or $d^{m\uparrow}s^{1\uparrow}d^{n+1\downarrow}s^{0\downarrow}$ (m $\geq$ 5) spin configurations. Due to the large band gap of BN, there is no charge transfer between TM and pristine SLBN, so all the TM atoms exhibit neutral charge states TM^0. This indicates that the magnetic properties of SLBN can be modified by adsorption of TM on its surface, as one would expect. Unfortunately, the calculations show that all TM atoms on SLBN have binding energies less than 1eV, agreeing with previous calculations[20], which indicates that the TM atoms on BN surface are quite mobile at room-temperature, like the diffusion of TM atoms on pristine graphene surface[21, 22].

As learned from TM/graphene system[10, 11, 21, 23], an effective way to enhance the stability of TM/SLBN system is to introduce defects in SLBN. These defects lead to a locally increased reactivity and thus enable the formation of stable chemical bonds with adsorbed atoms[21, 23, 24]. In experiments, vacancies and impurities (*e.g.* carbon and oxygen) are typically created during the synthesization of SLBN[14, 25, 26]. Taking boron-vacancy (V_B), nitrogen-vacancy (V_N), boron-nitrogen-vacancy (V_{BN}), and C-impurity as examples, we demonstrate here that charge and magnetic states of TM/SLBN can be easier controlled by defect engineering.

The (local) optimized structures of V_B, V_N, and V_{BN} are shown in Fig. 1a. In the case of V_B, the Jahn-Teller distortion lowers its symmetry from D_{3h} to C_{2v} after relaxation[28, 29]. The magnetic moments of N atoms at V_B are 1, 1, and -1 μ_B, respectively. The N-N distance between the two N atoms at V_B with opposite spin direction is 2.70 Å while the distance between the two N atoms with same spin direction is increased to 2.79 Å due to Coulomb repulsion. V_N has a symmetry of D_{3h} and the three first-neighbor B-B distances at V_N are

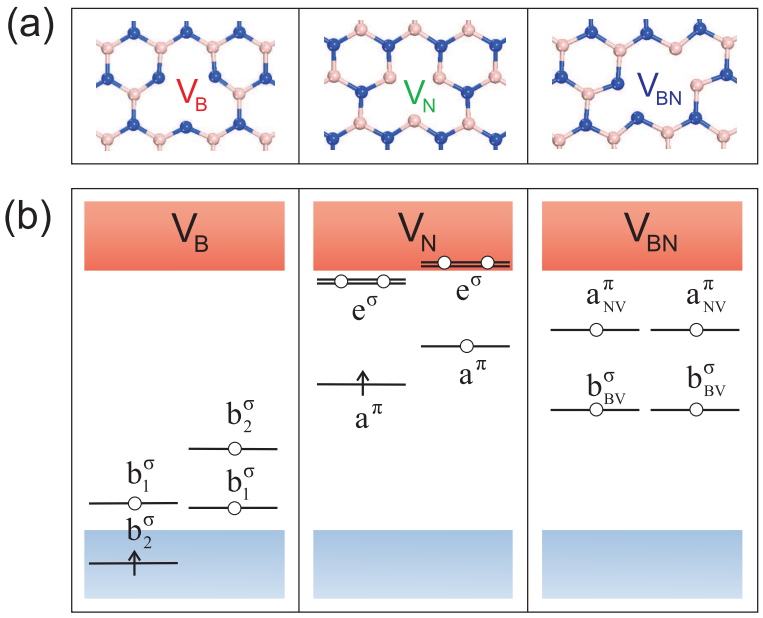

FIG. 1: (a) The (local) optimized geometries of V_B, V_N, and V_{BN} in SLBN. (b) The schematic drawings of the in-gap defect levels induced by V_B, V_N, and V_{BN}. The symmetry of these defect levels are explained in the text.

2.29 Å. The three B atoms at V_N have same spin directions and they contribute to a total magnetic moment of 1 μ_B. V_{BN} (C_{2v} symmetry) is spin-unpolarized. The first-neighbor B-B and N-N distances at V_{BN} are 1.93 and 1.81 Å, respectively.

The defect levels of V_B (V_N) at the vacancy site can be classified to have a^π, a^σ, e^π, and e^σ representations. In V_B, the a^π, a^σ, and e^π states are resonant inside the valence band while e^σ states are above the valence band maximum (VBM) in the gap. Due to the crystal field splitting caused by the Jahn-Teller distortion, the two-fold degenerate e^σ states further split into b_1^σ and b_2^σ, as shown in Fig. 1b. Finally, due to the spin exchange splitting, the occupied b_2^σ state in spin-up channel moves down into the valence band. The three hole levels above valence band make V_B acting as a triple-acceptor. Different from V_B, the a^π and e^σ levels derived from the B atoms at V_N site are present in the gap and e^σ is close to the conduction band minimum (CBM) and the a^π level in spin-up channel is occupied, as shown in Fig. 1b. The defect levels of V_{BN} could be regarded as the combination of V_B and V_N. Two unoccupied levels derived from B vacancy (b_{BV}^σ) and N vacancy (a_{NV}^π) at V_{BN} are present in the gap. The a_{NV}^π level is high in energy, making V_{BN} as a double-acceptor.

Depending on the position and symmetry of in-gap levels induced by vacancies, it is

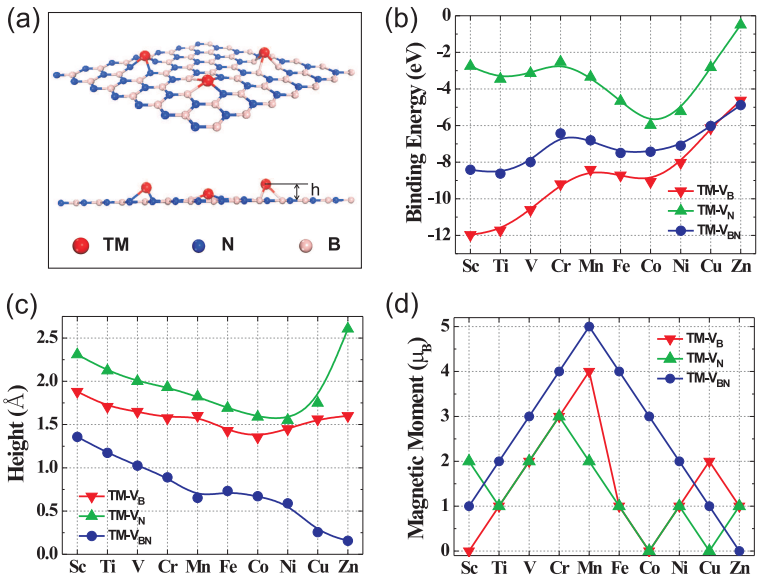

FIG. 2: (a) The schematic structure of TM atoms adsorb on V_B, V_N, and V_{BN} in SLBN. (b) The binding energies of TM atoms adsorption on V_B, V_N, and V_{BN} in SLBN. (c) The height of the TM atoms above the SLBN surface when TM atoms adsorb on V_B, V_N, and V_{BN}. (d) The magnetic moments of SLBN with TM atoms adsorption on V_B, V_N, and V_{BN}.

expected that they can interact with the adsorbed TM $3d$ to achieve the controllable charge and magnetic states of TM/SLBN. For instance, since the energies of TM $3d$ orbitals are roughly located at the middle of the gap of SLBN, they could behave as TM^{3+} ion after coupling to triple-acceptor V_B or TM^{2+} ion after interact with double-acceptor V_{BN}. Since the in-gap levels induced by V_N are comparable to that of $3d$ orbitals of TM in energy, instead of charge transfer, hybridization effect can play an critical role in determining the magnetic states of TM-V_N.

When a TM atom is attached on these vacancies (Fig. 2a), the binding energy of a TM atom on V_B (-4 $\sim$ -12 eV) is significantly larger than that of on V_{BN} and V_N, which could be understood by the larger charge transfer effect in TM-V_B. Among these TM atoms, Sc atom adsorption on V_B has the largest binding energy compared to other TM atoms on V_B, as shown in Fig. 2b, consisting with the fact that the $3d$ orbitals of Sc are highest in energy than other $3d$ TM atoms and the largest energy gain could occur for Sc/SLBN during the charge transfer.

For TM atoms adsorption on V_{BN}, two electrons of TM atom transfer to b^{σ}_{BV} level of V_{BN}, giving rise to TM^{2+} charge state. The alignment of the remaining $3d$ electrons exactly

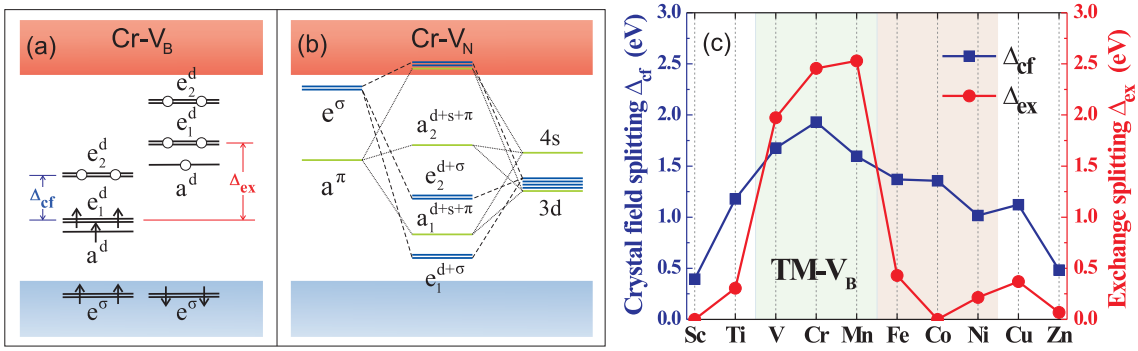

FIG. 3: (a) The schematic representation of the $3d$ levels of Cr atom after adsorption on V_B. The definition of the crystal field splitting Δ_{cf} and exchange splitting Δ_{ex} are explained in the text. (b) The schematic drawing of the symmetry-dependent coupling mechanism between V_N in-gap levels and Cr orbitals. (c) The calculated Δ_{cf} and Δ_{ex} of TM atoms in TM-V_B.

follows the Hund's rule, as shown in Fig. 2d. For TM atoms adsorption on V_B, TM atoms exactly exhibit TM^{3+} state after three electrons transfer to the three b^σ levels of V_B. Similar results are found for TM adsorption on cation-vacancy in other TM/III-V layers. All the TM atoms on V_B show high-spin configurations based on Hund's rule except for Fe, Co, and Ni atoms, as shown in Fig. 2d.

In order to understand the physical mechanism of the high-spin and low-spin configurations, we have analyzed the alignment and charge transfer between TM and SLBN. Taking Cr-V_B as a typical example of high-spin case, the $3d$ orbitals of Cr atoms are split into a single a^d (d_{z^2}) state and two 2-fold degenerate E_1^d ($d_{xy} + d_{x^2-y^2}$) and E_2^d ($d_{yz} + d_{xz}$) states under C_{3V} symmetry. E_1 and E_2 are mixed and split into two peaks, defined as e_1^d and e_2^d, as shown in Figs. 3a. After three electrons transfer to the V_B b^σ levels, the remaining d^3 orbitals of Cr^{3+} occupy the a^d and e_1^d in spin-up channel and exhibit a $d^{3\uparrow}d^{0\downarrow}$ high-spin configuration. The fully occupied V_B b^σ levels are then downshifted into valence band and convert to doubly degenerate e^σ state. In Cr-V_B, the size of exchange splitting of e^d orbitals Δ_{ex} is larger than that of crystal field splitting Δ_{cf} between e_1^d and e_2^d. The same physical mechanism results in the high-spin configurations in V-V_B and Mn-V_B. The case is opposite for the low-spin configurations in Fe-V_B, Co-V_B, and Ni-V_B, where $\Delta_{cf} > \Delta_{ex}$ (Fig. 3c). Taking Fe-V_B as an example, because $\Delta_{cf} > \Delta_{ex}$, the electrons transfer from e_2^d in spin-up channel to e_1^d in spin-down channel, resulting in a $d^{3\uparrow}d^{2\downarrow}$ low-spin configuration. The same physical mechanism results in the low-spin configurations of Co-V_B and Ni-V_B. Moreover,

because e^d is not occupied for Ti^{3+} while e_1^d in spin-down channel is fully occupied for Cu^{3+} and Zn^{3+}, the high-spin states of Ti-V_B, Cu-V_B, and Zn-V_B are not dependent on the relative sizes of $\Delta_{\rm cf}$ and $\Delta_{\rm ex}$. Generally, our results can be understood by the crystal field theory based on Griffith's theory of TM ions[27].

As we learned from the Cr-V_B and Fe-V_B cases above, the high or low spin configuration is mostly determined by the relative size of $\Delta_{\rm ex}$ and $\Delta_{\rm cf}$. Thus, the transition between high-spin and low-spin configurations of TM-V_B could be achieved by controlling the size of $\Delta_{\rm ex}$ and/or $\Delta_{\rm cf}$. To confirm our physical intuition, taking Fe-V_B as an example, our calculations show that if the height of Fe atom on V_B is increased from 1.42 Å to 1.61 Å (the total energy is increased by 0.23 eV), then $\Delta_{\rm cf} < \Delta_{\rm ex}$, and the spin of Fe transfers to the high-spin $d^{5\uparrow}d^{0\downarrow}$ configuration. In experiments, this spin transition might be achieved by either using a STM tip to modulate the height of TM atoms or applying a certain strain on SLBN.

The situation of TM atoms adsorption on V_N is more complicated and quite different from that of on V_B and V_{BN}. Since the position of V_N in-gap levels is comparable to that of TM $4s$, $3d$ orbitals in energy, the covalent hybridization between V_N a^π, e^σ and TM $4s$, $3d$ states plays the dominant role in determining the magnetic state of TM-V_N. TM s, d_{z^2} orbitals belong to the a representation under C_{3V} symmetry while TM $d_{xy,x^2-y^2,yz,xz}$ belong to the e representation. As shown in Fig. 1b, the in-gap levels of V_N also can be classified to a and e symmetry. According to the orbital selection rule, TM s, d_{z^2} orbitals mostly couple with V_N a^π state due to the same representation while TM $d_{xy,x^2-y^2,yz,xz}$ mostly couple with V_N e^σ states. Our electronic structure calculations confirm the orbital selection rule. Taking Cr-V_N as an example (Fig. 3b), the symmetry-dependent hybrid levels appear in the gap and are arranged in the order of $e_1^{d+\sigma}$, $a_1^{d+s+\pi}$, $e_2^{d+\sigma}$, $a_2^{d+s+\pi}$ in both spin-channels. The $e_1^{d+\sigma}$, $a_1^{d+s+\pi}$, $e_2^{d+\sigma}$ states are occupied in spin-up channel while only $e_1^{d+\sigma}$ is occupied in spin-down channel, giving rise to a magnetic moment of 3 μ_B. From Mn to Zn, the $a_1^{d+s+\pi}$ and $e_2^{d+\sigma}$ hybrid states become gradually occupied in spin-down channel as well, giving rise to low-spin configurations, as shown in Fig. 2d.

The general rule we provide here to control the charge and magnetic states of TM atoms by defect engineering is not limited to the vacancy defects but can be extended to other kinds of defects like C impurity. When C substitute N (C_N) in SLBN[25], because C is less electronegative than N, a defect level with C p_z component is pushed up above the valence band and it is occupied (unoccupied) in the spin-up (spin-down) channel[28, 30]. TM atom

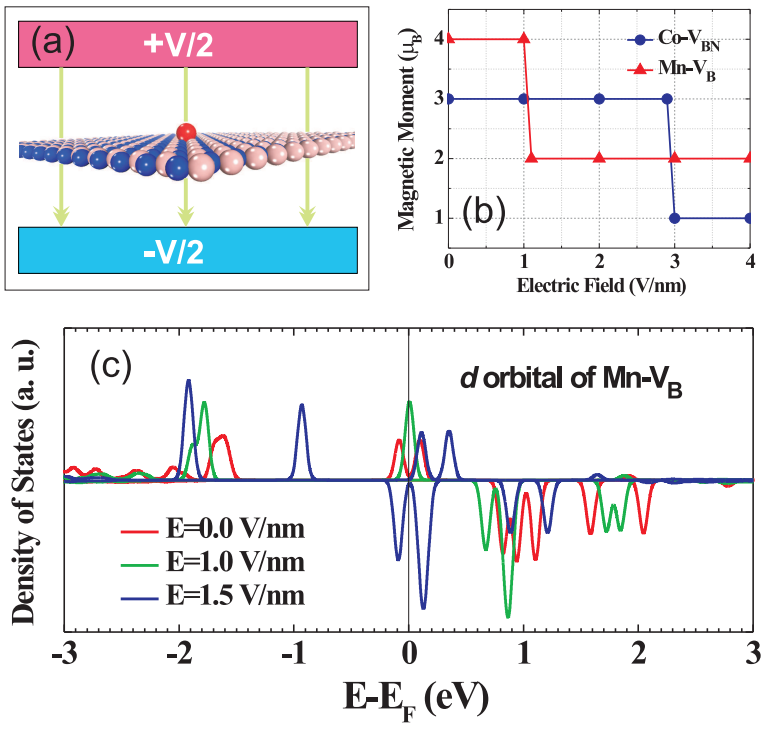

FIG. 4: (a) The model of a TM-SLBN system under an E_{ext}. An E_{ext} is oriented normally to SLBN surface and is assumed to be positive when it is directed downward. (b) The magnetic moments of Co-V_{BN} and Mn-V_B as a function of E_{ext}. (c) The energy shift of d orbitals for Mn-V_B as a function of E_{ext}. The Fermi level is set to zero.

on C_N transfers one electron to the unoccupied p-type defect level and exhibits TM^{1+} charge state. The remaining $3d$ orbitals of TM atoms are aligned as Hund's rule. For example, Mn on C_N exhibits an orbital alignment of $d^{5\uparrow}d^{1\downarrow}$ after one $4s$ electron transfers to $d^{\downarrow}$).

The understanding above suggests that the magnetic properties of TM/SLBN can be tuned if we can effectively adjust the relative energy positions of TM and/or defective SLBN. For example, applying an external electric field E_{ext} can shift the relative energy level positions because TM and SLBN are not in the same plane and because TM and SLBN can have opposite charge states when SLBN is defective. Taking Mn-V_B as an example (Fig. 4), Mn-V_B exhibits a $d^{4\uparrow}d^{0\downarrow}$ high-spin configuration without an E_{ext} (Fig. 2d). A positive E_{ext} exsert a force on the system, pushing the Mn closer to the SLBN becuase Mn is positive charged and SLBN is negatively charged. This increases the crystal field splitting. Remarkably, when E_{ext} is increased to 1.0 V/nm, the height of Mn atom on V_B is decreased suddenly from $\sim$ 1.6 /Å to $\sim$ 1.5 /Å. The large increase of the crystal field splitting causes

a spin-crossover, i.e., charges are transferred from the spin-up channel to the spin-down channel (Fig. 4c) and the spin configuration converts from $d^{4\uparrow}d^{0\downarrow}$ to $d^{3\uparrow}d^{1\downarrow}$, as shown in Fig. 4b. This low-spin state is found to be a metastable one with a total energy of $\sim$ 360 meV higher than that of the high-spin state in the absence of E_{ext}. Therefore, a negative critical E_{ext} is required to convert the low-spin state to high-spin one to realize the controllable spin-crossover effect.

The similar physical mechanism results in the spin configuration of Co-V_{BN} transfer from $d^{3\uparrow}d^{0\downarrow}$ to $d^{2\uparrow}d^{1\downarrow}$ when E_{ext} is about 3.0 V/nm (Fig. 4b). The fact that larger E_{ext} is required for the Co-V_{BN} system than the Mn-V_B system is consistent with the fact that the Co-V_{BN} is less ionized, i.e., less charge transfer between TM and SLBN, than Mn-V_B. It is worth to notice that the small critical E_{ext} in these systems indicates that it is possible to achieve this spin crossover effect in experiments[31]. Our calculations show that this spin crossover effect exists generally in TM/III-V and TM/II-VI layer structures, which strongly suggests that these TM/ionic-layer systems could be used for electromagnetic applications such as E_{ext}-driven non-volatile memory devices.

In conclusion, by using DFT calculations we have demonstrated that the charge and magnetic states of TM atoms on SLBN can be effectively controlled by internal defect engineering and external electric fields. Our conclusions got from TM/SLBN systems are valid in other TM/III-V or TM/II-VI layer structures.

B. H. and S.-H.W. acknowledge the support by the U.S. Department of Energy under Contract No. DE-AC36-08GO28308. J.Y. acknowledges the support by the National Research Foundation of Korea (No. R17-2008-033-01000-0). H. X. acknowledges the support by the National Science Foundation of China, Pujiang plan, and The Program for Professor of Special Appointment (Eastern Scholar) at Shanghai Institutions of Higher Learning.

---

[1] A. K. Geim and K. S. Novoselov, Nat. Mater. **6**, 183 (2007).

[2] M. Fujita, K. Wakabayashi, K. Nakada, and K. Kusakabe, J. Phys. Soc. Jpn. **65**, 1920 (1996).

[3] C. Tao, L. Jiao, O. V. Yazyev, Y. -C. Chen, J. Feng, X. Zhang, R. B. Capaz, J. M. Tour, A. Zettl, S. G. Louie, H. Dai, and M. F. Crommie, Nature Phys. **7**, 616 (2011).

[4] M. M. Ugeda, I. Brihuega, F. Guinea, and J. M. Gomez-Rodriguez, Phys. Rev. Lett. **104**,

096804 (2010).

[5] N. Tombros, C. Jozsa, M. Popinciuc, H. T. Jonkman, and B. J. van Wees, Nature **448**, 571 (2007).

[6] R. Sielemann, Y. Kobayashi, Y. Yoshida, H. P. Gunnlaugsson, and G. Weyer, Phys. Rev. Lett. **101**, 137206 (2008).

[7] V. W. Brar, R. Decker, H. Solowan, Y. Wang, L. Maserati, K. T. Chan, H. Lee, C. Girit, A. Zettl, S. G. Louie, M. L. Cohen, and M. F. Crommie, Nature Phys. **7**, 43 (2010).

[8] V. M. Karpan, G. Giovannetti, P. A. Khomyakov, M. Talanana, A. A. Starikov, M. Zwierzycki, J. van den Brink, G. Brocks, and P. J. Kelly, Phys. Rev. Lett. **99**, 176602 (2007).

[9] B. Uchoa, V. N. Kotov, N. M. R. Peres, and A. H. Castro Neto, Phys. Rev. Lett. **101**, 026805 (2008).

[10] A. V. Krasheninnikov, P. O. Lehtinen, A. S. Foster, P. Pyykko, and R. M. Nieminen, Phys. Rev. Lett. **102**, 126807 (2009).

[11] B. Huang, J. Yu, and S. -H. Wei, Phys. Rev. B **84**, 075415 (2011).

[12] D. D. Awschalom and M. E. Flatte, Nature Phys. **3**, 153 (2007).

[13] K. Sato, L. Bergqvist, J. Kudrnovsky, P. H. Dederichs, O. Eriksson, I. Turek, B. Sanyal, G. Bouzerar, H. Katayama-Yoshida, V. A. Dinh, T. Fukushima, H. Kizaki, and R. Zeller, Rev. Mod. Phys. **82**, 1633 (2010).

[14] K. K. Kim, A. Hsu, X. Jia, S. M. Kim, Y. Shi, M. Hofmann, D. Nezich, J. F. Rodriguez-Nieva, M. Dresselhaus, T. Palacios, and J. Kong, Nano Lett. **12**, 161 (2012).

[15] C. Tusche, H. L. Meyerheim, and J. Kirschner, Phys. Rev. Lett. **99**, 026102 (2007).

[16] C. L. Freeman, F. Claeyssens, N. L. Allan, and J. H. Harding, Phys. Rev. Lett. **96**, 066102 (2006).

[17] D. Wu, M. G. Lagally, and F. Liu, Phys. Rev. Lett. **107**, 236101 (2011).

[18] W. A. Harrison, *Electronic Structure and The Properties of Solids*, Dover publications, 1989.

[19] The calculation details can be found in the Supplemental Material.

[20] C.Ataca and S. Ciraci, Phys. Rev. B **82**, 165402 (2010).

[21] Y. Gan, L. Sun, and F. Banhart, Small **4**, 587 (2008).

[22] R. Zan, U. Bangert, Q. Ramasse, and K. S. Novoselov, Nano Lett. **11**, 1087 (2011).

[23] O. Cretu, A. V. Krasheninnikov, J. A. Rodriguez-Manzo, L. Sun, R. M. Nieminen, and F. Banhart, Phys. Rev. Lett. **105**, 196102 (2010).

[24] M. Gyamfi, T. Eelbo, M. Wasniowska, and R. Wiesendanger, Phys. Rev. B **84**, 113403 (2011).

[25] O. L. Krivanek, M. F. Chisholm, V. Nicolosi, T. J. Pennycook, G. J. Corbin, N. Dellby, M. F. Murfitt, C. S. Own, Z. S. Szilagyi, M. P. Oxley, S. T. Pantelides, and S. J. Pennycook, Nature **464**, 571 (2010).

[26] C. Jin, F. Lin, K. Suenaga, and S. Iijima, Phys. Rev. Lett. **102**, 195505 (2009).

[27] J. S. Griffith, *The Theory of Transition-metal Ions*, Cambridge university press, 1961.

[28] S. Azevedo, J. R. Kaschny, C. M. C. de Castilho, and F. de Brito Mota, Eur. Phys. J. B **67**, 507 (2009).

[29] C. Attaccalite, M. Bockstedte, A. Marini, A. Rubio, and L. Wirtz, Phys. Rev. B **83**, 144115 (2011).

[30] N. Berseneva, A. V. Krasheninnikov, and R. M. Nieminen, Phys. Rev. Lett. **107**, 035501 (2011); B. Huang and S. -H. Wei, Phys. Rev. Lett. **107**, 239601 (2011).

[31] Y. Zhang, T. -T. Tang, C. Girit, Z. Hao, M. C. Martin, A. Zettl, M. F. Crommie, Y. R. Shen, F. Wang, Nature **459**, 820 (2009).